

# Theory of Highly Directional Emission from a Single Subwavelength Aperture Surrounded by Surface Corrugations

L. Martín-Moreno,<sup>1</sup> F. J. García-Vidal,<sup>2</sup> H. J. Lezec,<sup>3</sup> A. Degiron,<sup>3</sup> and T.W. Ebbesen<sup>3</sup>

<sup>1</sup>Departamento de Física de la Materia Condensada, ICMA-CSIC, Universidad de Zaragoza, E-50009 Zaragoza, Spain

<sup>2</sup>Departamento de Física Teórica de la Materia Condensada, Universidad Autónoma de Madrid, E-28049 Madrid, Spain

<sup>3</sup>ISIS, Université Louis Pasteur, 67000 Strasbourg, France

(Received 16 July 2002; published 23 April 2003)

We present a theoretical foundation for the beaming of light displayed by a single subwavelength aperture in an appropriately corrugated metal film [H. J. Lezec *et al.*, Science **297**, 820 (2002)]. Good agreement is found between calculations and experimental data. We show that beaming is due to the formation of electromagnetic surface resonances and that the beam direction, width, and wavelength at which it occurs can be selected by tuning geometrical parameters of the structure.

DOI: 10.1103/PhysRevLett.90.167401

PACS numbers: 78.66.Bz, 42.79.Dj, 71.36.+c, 73.20.Mf

Light emerging from a subwavelength aperture is normally fully diffracted in all directions. Very recently, it has been shown that this radiation pattern could be compressed into a narrow beam by patterning the surface immediately surrounding the exit plane of the aperture [1]. These patterns typically consist of a periodic set of shallow grooves in a metal surface. One of the surprising features of this phenomenon is the combination of a radiating area strongly confined to the vicinity of the aperture and a small angular divergence of the emitted light. This effect offers exciting possibilities for novel applications, adding to the rich variety of optical phenomena displayed by nanostructured metallic systems [2–10]. Reference [1] presented a phenomenological model for the beaming effect which assumed an electromagnetic leaky mode running along the exit surface, mode interpreted as the surface plasmon of the corrugated metal. The position dependent intensity of this wave and its dispersion relation were unknown and fitted to match experimental data. While this model provided good fits to the experimental results, it was based on a number of empirical parameters and its range of validity was not clear.

Here we present a first-principles theoretical framework which gives good agreement with the experimental results, describes the beaming mechanism in detail, and provides support to the phenomenological model of Ref. [1]. Results will be presented mainly for *p* polarization (*E* field perpendicular to the grating symmetry plane), as beaming is experimentally observed only in this case.

We study the angular distribution of light after passing through an opaque metal film with a single narrow slit (slit width, *a*, smaller than the electromagnetic (EM) wavelength,  $\lambda$ ), surrounded by a certain number of one-dimensional (1D) grooves. The grooves may be patterned on either metal surface or on both. The total transmittance  $T(\lambda)$  depends on the angle of incidence and all parameters defining the metal corrugation. However, we have found that, for  $a \ll \lambda$ , the angular distribution of the

transmitted light [represented by the normalized-to-transmittance Poynting vector  $\tilde{S}^{\text{nor}}(\lambda, \vec{r}) = \tilde{S}(\lambda, \vec{r}) / T(\lambda)$ ] depends only on properties of the output surface. As this Letter deals with how light is spatially distributed and not with how much is transmitted, we focus on  $\tilde{S}^{\text{nor}}(\lambda, \vec{r})$  for the geometry depicted in Fig. 1(a), for a wave with amplitude  $A_0$  approaching the output surface from the central slit.

In order to discuss in the simplest possible terms the mechanisms involved in the rich emission profiles, we apply perfect metal boundary conditions, and consider

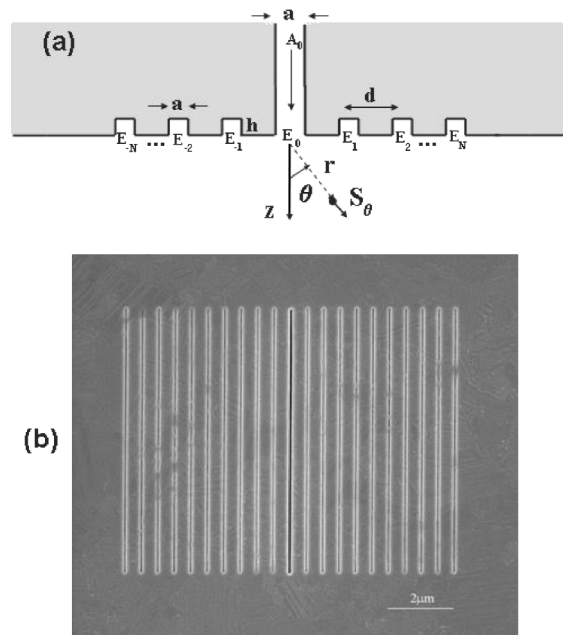


FIG. 1. (a) Schematic picture for the system analyzed: single slit surrounded in the exit surface by a finite array of grooves. In this paper all indentations have width *a*, and grooves have depth *h*. (b) Focused-ion-beam image of the exit surface of a slit in a Ag film, with  $N = 10$  grooves at each side, and nominal values  $a = 40$  nm,  $d = 500$  nm, and  $h = 100$  nm.

only the fundamental mode in both slit and grooves. For good metals, such as gold or silver, comparisons with fuller calculations performed in related systems [7,11] support these two approximations which, as will be shown here, are enough to explain all experimental beaming features.

Calculations are performed by considering a supercell of the system, with cell parameter  $L$ , expressing the fields in different regions in terms of their mode expansion, matching the fields appropriately on all interfaces, and taking  $L \rightarrow \infty$ . For  $p$ -polarized light this leads to the following set of equations for the unknowns  $E_\alpha$ :

$$[G_{\alpha\alpha} - \epsilon_\alpha]E_\alpha + \sum_{\beta \neq \alpha} G_{\alpha\beta}E_\beta = 2iA_0\delta_{\alpha 0}, \quad (1)$$

$\alpha$  and  $\beta$  running over all indentations (slit or grooves).  $E_\alpha$  is related to the  $x$  component of the electric field at  $z = 0^-$  through  $E_x(z = 0^-) = \sum_\alpha E_\alpha \phi_\alpha(x)$ , with  $\phi_\alpha(x) = 1/\sqrt{a}$  at the opening  $\alpha$  and 0 otherwise.  $\epsilon_\alpha = \cot(kh)$  at the grooves ( $a \neq 0$ ), while  $\epsilon_0 = -i$ , and  $G_{\alpha\beta}$  is a Green's function projected over modes  $\phi_\alpha$  and  $\phi_\beta$ :  $G_{\alpha\beta} = ik/2 \int \phi_\alpha^*(x)\phi_\beta(x')H_0^{(1)}(k|x-x'|)dx dx'$ , where  $k = 2\pi/\lambda$  and  $H_0^{(1)}(x)$  is first-kind Hankel's function [12].

From  $E_\alpha$ , we obtain  $T(\lambda) = |A_0|^2 - |A_0 - E_0|^2$  and the magnetic field in the  $z > 0$  region as

$$H_y(\vec{r}) = \frac{1}{\mu_0 c} \sum_\alpha E_\alpha G(\alpha, \vec{r}); \quad (2)$$

all other components of the EM field can be obtained from  $H_y(\vec{r})$  for the polarization considered. Here  $G(\alpha, \vec{r}) = (ik/2) \int \phi_\alpha^*(x)H_0^{(1)}(k|x\hat{u}_x - \vec{r}|)dx$ .

These equations have a clear physical interpretation. Equation (1) is a tight-binding-like equation governing the wandering of the EM field between indentations, for a given “external illumination” coming from the central slit,  $A_0$ . The term  $G_{\alpha\beta}E_\beta$  gives the radiation that, emitted by indentation  $\beta$ , reaches indentation  $\alpha$ . As Eq. (2) shows, for the emission profiles, a system of a narrow slit and a collection of grooves behave like an equivalent diffraction grating of narrow 1D emitters [13]. However, the equivalent diffraction grating is very peculiar: as we will show, the EM field amplitudes at the emitters (the  $E_\alpha$ 's) present a strong dependence on distance to the slit and  $\lambda$ , and must be solved self-consistently from Eq. (1).

We consider a symmetric structure with  $\pm N$  grooves on each side of the slit with, unless otherwise stated, geometrical parameters being those of the device rendered in Fig. 1(b). The calculated and experimental far-field angular transmission distributions [14] can be seen in the insets of Fig. 2. Apart from a rigid blueshift of  $\approx 15$  nm [see inset (L)], and an overestimation of the maximum beaming attainable [inset (R)], our simple model reproduces well the experimental data. Notice that no attempt has been made here to fit the experimental data, so no adjustable parameter enters in the comparison.

Consider now the dependence of  $I_N(\theta) = rS_\theta^{\text{nor}}(\theta)$  with number of grooves,  $N$ . Curves for  $N = 0$  in Figs. 2(a) and 2(b) correspond to the single slit case where, as  $a \ll \lambda$ ,  $I_0(\theta) \approx 1/\pi$ , practically independent of both  $\theta$  and  $\lambda$ . For  $\lambda = 560$  nm, as  $N$  increases a very strong narrow peak develops at  $\theta = 0$ . A smooth maximum in  $I_N(0)$  occurs for  $N = 7$  [when  $I_7(0) \approx 10I_0(0)$ ], showing that beaming intensity does not necessarily increase when increasing  $N$ . At other  $\lambda$ , the beaming intensity is not so strong but  $I(\theta)$  does not saturate for such small values of  $N$ , as shown in Fig. 2(b) for the representative case  $\lambda = 800$  nm. For  $s$  polarization, a similar calculation gives that adding grooves to the central slit changes  $I(\theta)$  by about 10% in the best of cases, in keeping with the lack of beaming found in the experiments for this case.

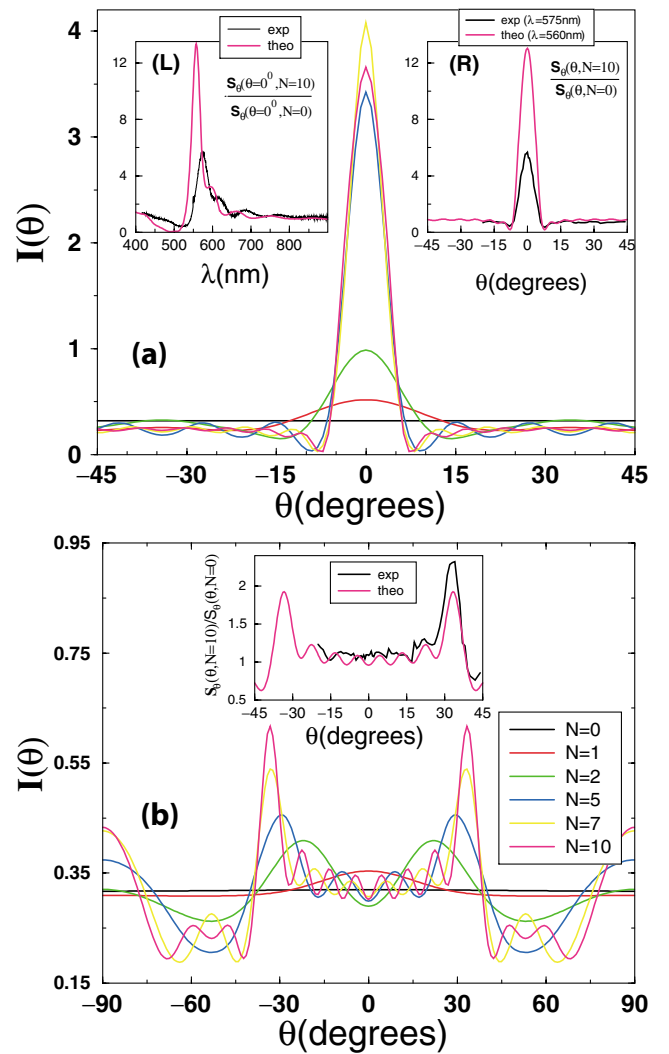


FIG. 2 (color). Calculated angular transmission distribution,  $I_N(\theta)$ , for  $\pm N$  grooves surrounding a central slit. Geometrical parameters as in Fig. 1(b). (a)  $\lambda = 560$  nm; (b)  $\lambda = 800$  nm. Insets show the comparison between measured and calculated  $\Delta S(\theta) = S_\theta(\theta, N = 10)/S_\theta(\theta, N = 0)$ . (L):  $\Delta S(0)$  vs  $\lambda$ . (R):  $\Delta S(\theta)$  at maximum forward beaming ( $\lambda^{\text{theo}} = 560$  nm,  $\lambda^{\text{exp}} = 575$  nm). Inset to (b):  $\Delta S(\theta)$  for  $\lambda = 800$  nm.

The dependence of  $I(\theta)$  on  $\lambda$  is summarized in Fig. 3. Note that the  $\lambda$  at which maximum beaming occurs shifts with  $h$ . Also the maximum attainable beam intensity is a strong function of  $h$ : for small  $h$  beaming intensity is small [note the change in color scale from Fig. 3(a) to Figs. 3(b) and 3(c)], being close to optimal for  $h = 100$  nm and decreasing for larger  $h$ .

It is clear from Eq. (2) that the observed beaming is an interference phenomena for which a necessary condition is that  $E_\alpha$  must be appreciable at several indentations. The formation of  $E_\alpha$  and the emission process can be visualized as follows: the output side of the slit diffracts a primary beam into vacuum and (through evanescent modes) into the grooves. The grooves may, in turn, diffract radiation either to vacuum or into other indentations.

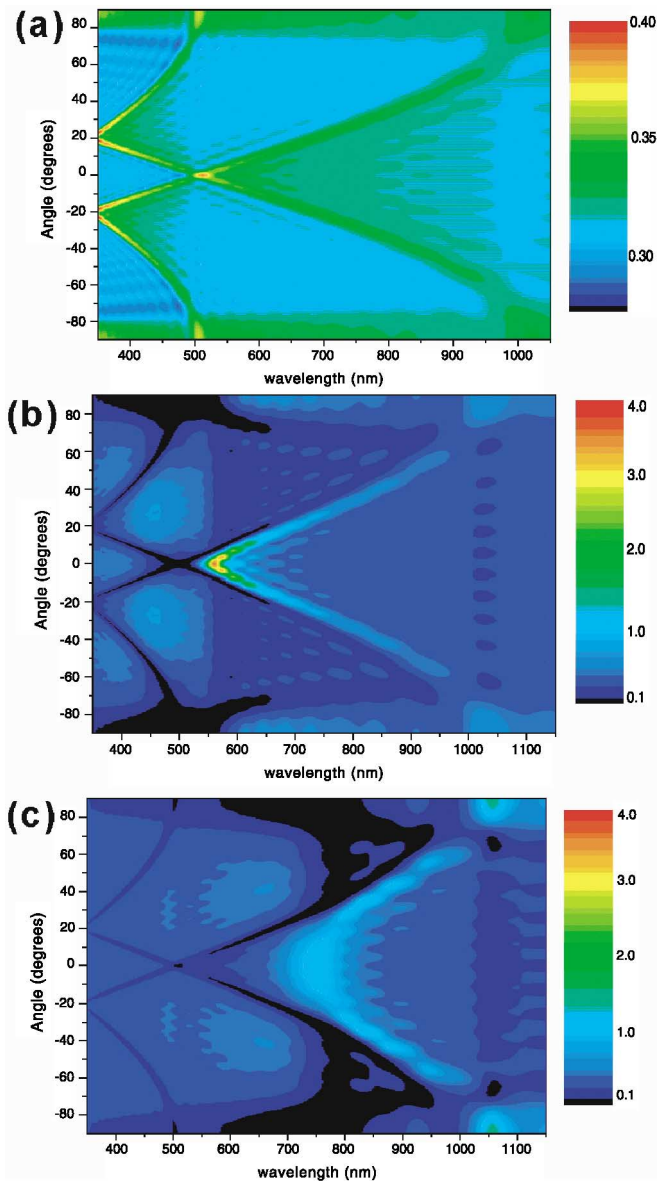


FIG. 3 (color). Contour plots for  $I(\lambda, \theta)$  for three different groove depths, other geometrical parameters ( $a, d, N$ ) as in Fig. 1(b). (a)  $h = 10$  nm, (b)  $h = 100$  nm, (c)  $h = 160$  nm.

Eventually, an EM field is self-consistently built up at the output surface while light is reemitted into vacuum. This view suggests a family of approximations to Eq. (1). In zero order only direct illumination into the slit is considered. The first order takes into account, additionally, radiation diffracted from the slit into the grooves, ignoring reradiation from them. In general, fields in the  $n$ th order approximation,  $E_\alpha^{(n)}$ , can be written as

$$[G_{\alpha\alpha} - \epsilon_\alpha]E_\alpha^{(n)} = - \sum_{\beta \neq \alpha} G_{\alpha\beta}E_\beta^{(n-1)} + 2iA_0\delta_{\alpha 0}. \quad (3)$$

For a given set of  $\lambda$  and geometrical parameters, approximations of different orders are required to match the exact results, reflecting the degree of importance of reradiation from the grooves. Actually the iterative solution to Eq. (3) may not converge for some ranges of  $\lambda$ ; then the graphical picture of EM fields hopping repeatedly fails, and must be replaced by the, always correct, self-consistent formation of EM fields described by Eq. (1). While the first-order approximation could have been inferred by simple diffraction arguments [15], we associate the nonconvergence of iterative solutions to Eq. (3) to the formation of EM surface resonances. Note that surface modes appear even in corrugated *perfect* metal structures. This occurs because indentations provide a region close to the surface where electric and magnetic fields are now possible; i.e., they provide an effective impedance,  $Z^{\text{eff}}$ , to the surface. The impedance  $Z_\alpha$  for an isolated narrow groove is  $Z_\alpha^{-1} = i\epsilon_\alpha$  which, spatially averaged in the case of a periodic system of grooves gives  $Z^{\text{eff}} = -i(a/d)\tan(kh)$ . For some ranges of  $kh$ ,  $\text{Im}Z^{\text{eff}} < 0$ , as would correspond to a flat *real* metal surface, opening the possibility for surface modes, which can be interpreted as the surface plasmons of this effective medium. These are leaky modes (resonances), as they couple to radiative modes. Considering this coupling provides a real part to  $Z^{\text{eff}}$ , in much the same way as  $\text{Im}\epsilon(\omega)$  takes into account the EM energy transferred to non-EM degrees of freedom. This effective medium view is further supported as, for  $s$  polarization, the outlined procedure leads to a positive imaginary  $Z^{\text{eff}}$ , so the corrugated perfect metal surface cannot be seen as an effective metal one and surface modes do not appear.

Angular transmission profiles are well described by the diffractionlike first-order approximation if  $|E_\alpha| \ll |E_0|$ , which occurs for  $h \ll \lambda$ , when  $\epsilon_{\alpha \neq 0} \gg 1$ ; a representative case is shown in Fig. 3(a) ( $h = 10$  nm). In this case,  $E_0 \approx 2iA_0/(G_{00} - \epsilon_0)$  and  $E_\alpha \approx -G_{\alpha 0}E_0/(G_{\alpha\alpha} - \epsilon_\alpha)$ . From the asymptotic expansion of  $H_0^1(kx)$ ,  $|E_\alpha| \sim \alpha^{-1/2}$ , while the phase of  $E_\alpha$  is  $\phi_\alpha = kd|\alpha| + \phi$  for grooves and a value  $\phi_0$ , not following the previous law, for the slit. The origin of the beaming at angles  $\theta_F^{(m,\pm)}(\lambda) = \arcsin(m\lambda/d \pm 1)$  (for integer  $m$ ) shown in Fig. 3(a) is that, as the phase difference for grooves at one side of the slit is constant, it can be canceled in the far field at those angles. Therefore, in an asymmetric structure (with grooves on just one side of the slit) only either  $\theta_F^{(m,+)}$  or

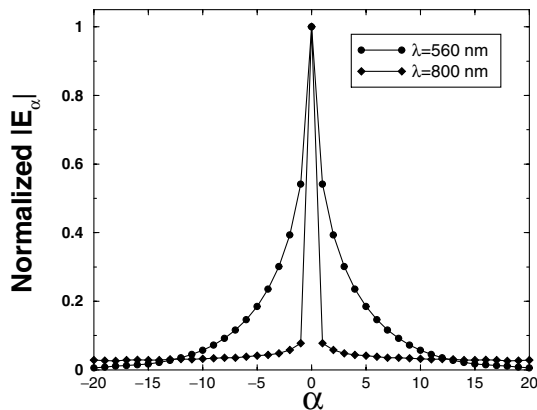


FIG. 4. Dependence of  $|E_\alpha|$  with distance to the central slit for two different  $\lambda$ . Geometrical parameters as in Fig. 1(b), except that here  $N = 20$ , to show clearly the dependence on  $\alpha$ .

$\theta_F^{(m,-)}$  would appear, depending on which side had been patterned.

As  $h$  increases,  $\epsilon_\alpha$  approaches  $G_{\alpha\alpha}$ , and higher order approximations may be needed. Indeed, close to the single groove cavity resonance condition,  $\text{Re}(G_{\alpha\alpha} - \epsilon_\alpha) = 0$ , we find collective modes. Since in each hop light is partially reradiated into vacuum, with an intensity proportional to  $|E_\alpha|^2$ , high-order processes quickly decay, implying intense emitters strongly localized close to the slit. This is illustrated in Fig. 4, showing the dependence of  $|E_\alpha|$  with  $\alpha$ , for the cases considered in Fig. 2. For this set of geometrical parameters, the groove cavity resonance occurs at  $\lambda_R = 512$  nm. For  $\lambda = 560$  nm [Fig. 2(a)],  $|E_\alpha|$  presents the described typical dependence of a collective surface mode, explaining both the intense beaming and the saturation at small  $N$  found in Fig. 2(a). On the contrary, for  $\lambda = 800$  nm,  $E_\alpha$  is well represented by a low order approximation, so the EM field is smaller at the grooves and decays more slowly, explaining why the beaming intensity found in Fig. 2(b) is not that strong and depends on  $N$ . Notice that, even for maximum beaming conditions, the EM energy density at indentation  $\alpha$  (proportional to  $|E_\alpha|^2$ ) has strongly decayed already at the slit next-nearest neighbor grooves. Therefore, the emitting area is much smaller than the total area covered by indentations [point we have corroborated by explicit calculation of  $S_z(\vec{r})$ ], in agreement with experiment [1].

Calculations show that the linearity of  $\phi_\alpha$  with  $\alpha$ , exact for first-order processes, still holds to a good approximation even when higher order processes are important. This is why special beaming properties are found in Figs. 3(b) and 3(c) at the angles  $\theta_F(\lambda)$  predicted by simple diffraction. But,  $I(\theta_F)$  may be enhanced or suppressed, depending on the phase relation between radiation from the grooves and from the slit. For example, in the system described in Fig. 2, as high  $|E_\alpha|$ 's are expected for  $\lambda \approx \lambda_R = 512$  nm, strong far-field beaming could naively be expected at  $\theta = 0$  for  $\lambda = d = 500$  nm, where

beams from all grooves are in phase. However, at  $\lambda = 500$  nm, these beams are in phase opposition to the slit contribution, finally producing a minimum in  $I(\theta = 0)$ . As  $\lambda$  crosses  $\lambda_R$ ,  $(G_{\alpha\alpha} - \epsilon_\alpha)$  changes sign, producing a strong variation of all  $\phi_{\alpha \neq 0}$ . Maximum beaming occurs at a  $\lambda > \lambda_R$  (in this case at  $\lambda = 560$  nm), when beams from the slit and grooves are approximately in phase at  $\theta = 0$ .

Another factor that favors surface modes (and therefore high  $|E_\alpha|$  and intense beaming) is  $\lambda$  being commensurate with  $d$ , so reradiated light from the grooves reach other grooves in phase. This is illustrated in Fig. 3(c), where beaming properties can be explained following the previous discussion. Only, this time maximum beaming occurs around  $\lambda_R = 700$  nm and, as this condition is farther away from the  $\lambda = d$  resonant reemission condition, beaming is not as intense as for the  $h = 100$  nm case.

In conclusion, we have presented a theoretical study of the beaming properties of a single subwavelength slit in a metal surface surrounded by a finite array of grooves, obtaining good agreement with experimental data. We have shown that beaming properties are due to the formation of EM surface resonances. These resonances result from the combination of single groove cavity modes (controlled by groove depth and width) and the coupling between indentations (which is maximum at wavelengths commensurate with the period). The wavelength at which beaming occurs, the beam width and the direction of light can be selected by just tuning geometrical parameters. These features make such structures excellent candidates for all-optical and optoelectronic devices. Moreover, these devices need not be large since strong beaming can be achieved with emission regions of dimensions comparable to the wavelength.

- [1] H. J. Lezec *et al.*, Science **297**, 820 (2002).
- [2] W. L. Barnes *et al.*, Phys. Rev. B **51**, 11164 (1995).
- [3] T. W. Ebbesen *et al.*, Nature (London) **391**, 667 (1998).
- [4] V. A. Shubin *et al.*, Phys. Rev. B **62**, 11230 (2000).
- [5] E. Popov *et al.*, Phys. Rev. B **62**, 16100 (2000).
- [6] L. Salomon *et al.*, Phys. Rev. Lett. **86**, 1110 (2001).
- [7] L. Martín-Moreno *et al.*, Phys. Rev. Lett. **86**, 1114 (2001).
- [8] S. I. Bozhevolnyi *et al.*, Phys. Rev. Lett. **86**, 3008 (2001).
- [9] J. R. Sambles, Phys. Rev. Lett. **89**, 063901 (2002).
- [10] E. Altewischer, M. P. Van Exter, and J. P. Woerdman, Nature (London) **418**, 304 (2002).
- [11] F. J. García-Vidal and L. Martín-Moreno, Phys. Rev. B **66**, 155412 (2002).
- [12]  $G_{\alpha\beta}$  originates from a sum of all diffracted waves:  $G_{\alpha\beta} = (\imath/\pi) \int [\sin(k_x a/2)/(k_x a/2)]^2 e^{ik_x d(\alpha-\beta)} k / \sqrt{k^2 - (k_x)^2} dk_x$ .
- [13] In retrospect, this Huyghen's-principle-like result is why  $\tilde{S}^{\text{nor}}(\lambda, \vec{r})$  does not depend on input corrugation.
- [14] The effect of the small finite collection angle of the detector has been included.
- [15] J. M. Vigoureux, Opt. Commun. **198**, 257 (2001).